Available online at www.sciencedirect.com
ScienceDirect
Polymer 47 (2006) 7580–7589
polymer
www.elsevier.com/locate/polymer

Heterogeneous nucleation uniformizing cell size distribution in microcellular nanocomposites foams

Wentao Zhai [a,b], Jian Yu [a,*], Lichuan Wu [a,b], Weiming Ma [a,b], Jiasong He [a,*]

[a] *Beijing National Laboratory for Molecular Sciences (BNLMS), Key Laboratory of Engineering Plastics, Joint Laboratory of Polymer Science and Materials, Institute of Chemistry, Chinese Academy of Sciences, Beijing 100080, China*
[b] *Graduate School, Chinese Academy of Sciences, Beijing 100039, China*

Received 13 February 2006; received in revised form 10 August 2006; accepted 17 August 2006
Available online 7 September 2006

Abstract

Microcellular polycarbonate/nano-silica nanocomposites (PCSN) were prepared by temperature rising process using supercritical CO_2 as the blowing agent. Neat PC foam showed a quite broad distribution of cell sizes. Under the same foaming conditions, the addition of nano-silica resulted in PCSN foams having uniform cell size distribution, reduced cell size of 0.3–0.5 μm and increased cell density of 10^{11}–10^{13} cells/cm^3. The underlying nucleation mechanism was semi-quantitatively analyzed by the classical nucleation theory. The results indicate that the energy-barrier for heterogeneous nucleation was three orders of magnitude lower than that of homogeneous one. The heterogeneous nucleation of nano-silica aggregates dramatically increased the nucleation rate, decreased the nucleation time interval, and hence facilitated the almost instantaneous growth of cell size. Combined with the well-dispersed nucleation sites, resulted from the uniform dispersion of nano-silica aggregates, the narrow-distributed cell size was obtained in PCSN foams.

Keywords: Microcellular foam; Heterogeneous nucleation; Polycarbonate

1. Introduction

Polymeric foams have been widely used in many applications because of their high strength-to-weight ratio, excellent heat and sound insulations, high energy or mass absorption, and materials saving, etc [1]. In early 1980s [2], a concept of microcellular foams was developed with several advantages. With cell size smaller than 10 μm, microcellular foams can reduce significantly the amount of plastics used while improve some mechanical properties, and may offer special properties which are not possessed by the conventional foams and the unfoamed polymers. To obtain polymeric microcellular foam with desirable cell size, the process typically requires higher nucleation rates and higher inert gas concentrations than the conventional processes. The additives, generally micron-sized inorganic particles, were employed as nucleating agents to induce heterogeneous nucleation for producing a large number of nucleation sites in the early efforts [3–8]. McClurg [9] outlined the qualities of ideal nucleants for polymer foaming and suggested that the large amount of uniformly dispersed particles with uniform size and non-wetting surface would be the suitable nucleating agents to produce desirable foams with high cell density and small cell size. More recent studies have focused on the production of microcellular foams with high cell density (>10^9 cells/cm^3) by using nano-scaled nucleating agents, of which organically modified layered silicates were the most commonly used [11–17]. Cylindrical [10,18] and spherical [19,20] nanoparticles were also used for microcellular foaming. The homogeneous nanoparticle dispersion, favorable surface property and particle geometry account for the significant increase in cell density and decrease in cell diameter by adding a small amount of nanoparticles [10].

* Corresponding authors. Tel.: +86 10 62613251; fax: +86 10 82612857.
E-mail addresses: yuj@iccas.ac.cn (J. Yu), hejs@iccas.ac.cn (J. He).

0032-3861/$ - see front matter © 2006 Elsevier Ltd. All rights reserved.
doi:10.1016/j.polymer.2006.08.034

Moreover, the cell size distribution is another important parameter to characterize the cell morphology in polymer foam, which has a significant effect on the physical and mechanical properties of foams along with the cell size and cell density. It was indicated by Shafi et al. [23] that the most sensitive parameters to finalize cell size distribution were those associated with the nucleation process, such as the blowing agent concentration and Gibbs free energy. Non-uniform distribution of temperature, gas pressure, and gas concentration in polymer system, as well as a secondary nucleation process, can result in a broad cell size distribution because the cells do not generate simultaneously [21,22]. Therefore, shortening of the nucleation time interval is a main means to obtain narrow cell distribution in microcellular foams. An increase in cell nucleation rate obviously decreases the time interval for nucleation process, and is expected to narrow the cell size distribution of the final foam [24]. On the other hand, the heterogeneous nucleation induced by the nucleating agents, especially nano-scaled nucleating agents, decreases dramatically the energy-barrier for cell nucleation, increases the cell nucleation rate, and is expected to narrow the cell size distribution as well. However, as far as we are concerned, no experimental evidence has been reported to reveal the effect of nucleating agent with nano-scale size on the cell size distributions of microcellular foams, mostly because of the lack of suitable pure polymer system having a broad cell size distribution. Up to now, most microcellular foams of pure polymers exhibit relatively narrow cell size distribution by using supercritical fluid technology.

In our present study, neat melt-processed polycarbonate (PC) was found unexpectedly to exhibit a broad distribution of cell sizes by microcellular foaming of supercritical CO_2 ($scCO_2$), which was undoubtedly suitable as control to study the nucleation behavior of nano-sized nucleating agent. The spherical nano-silica was chosen as the nucleating agent, and microcellular PC nanocomposites were prepared by melt blending, followed by foaming via a temperature rising process. Here the influence of nano-sized nucleating agent on the nucleation process and the cell size distribution of final foams were investigated under different nano-silica contents, saturation pressures, foaming temperatures, and foaming times. A discussion, based on the classical nucleation theory, was focused on the nucleation energy of the homogeneous and heterogeneous nucleations, and the nucleation efficiency of nano-silica.

2. Experimental section

2.1. Materials

PC (Makrolon 3208) was supplied as granules by Bayer. Nano-silica (Aerosil R974) with a primary particle size of 12 nm was obtained from Degussa, Germany, having the surface modified with 1,1-dimethyl-dichlorosilane by the manufacturer. All these materials were dried in vacuum at 100 °C for at least 24 h before use. CO_2 with a purity of 99.95% was supplied by Beijing Analytical Gas Factory.

2.2. Nanocomposite preparation

Nano-silica filled PC with 9 wt% silica loading was prepared first as a master batch using a twin-screw extruder (Haake RC90 TW100) with a temperature profile of 260–275–285–275 °C from the hopper to die. The screw speed was 60 rpm. The resultant composite was further processed or diluted with PC in a batch mixer (Haake RC90 Rheomix 600) at 280 °C. The mixing time was 6 min and the rotator speed was 60 rpm. A series of composites with silica content of 1, 3, 5, and 9 wt% obtained were hereafter coded as PCSN1, PCSN3, PCSN5, and PCSN9, respectively. For comparison, neat PC was also processed with the mixer under the same conditions. After being dried at 100 °C under vacuum for 24 h, the processed samples as well as the as-received PC were compression molded into sheets with 1 mm thickness at 260 °C. The sheets were cut into the specimens with dimensions of 5 × 25 mm for batch foaming.

2.3. Batch foaming

PC can be induced to crystallize by $scCO_2$ under certain conditions [25–27]. The presence of crystalline region will affect the cell nucleation and growth process in the course of foaming [28,29]. Therefore, all samples were saturated with CO_2 in a vessel at 50 °C and CO_2 pressure of 12–20 MPa to avoid PC crystallization. The saturation time was 10 h to ensure equilibrium adsorption of CO_2. Subsequently, these samples were removed from the vessel after a rapid quench of pressure, and transferred to a glycerin bath kept at a scheduled temperature (100–150 °C) within a 1 min interval. Samples were immersed in the glycerin bath for 30 s unless indicated. Then the foamed samples were quenched with cold water.

2.4. Characterization

Gel permeation chromatography (GPC) measurements were carried out with a Waters 510 GPC instrument at 40 °C, and the mobile phase was chloroform with a flow rate of 1 mL/min. The mass densities of samples before (ρ) and after foaming treatment (ρ_f) were determined via water displacement method according to ISO 1183-1987. The uptake of water by the sample can be neglected during the measurement due to smooth skin and closed cells of the foamed sample. The dispersion and actual size of nano-silica in the PC domain were characterized by transmission electron microscopy (TEM). Samples were microtomed in liquid nitrogen with a diamond knife and mounted on a 200-mesh copper grid. Images were obtained from a Philips CM12 apparatus using an accelerating voltage of 80 kV. The morphology of solid composites and foamed samples was observed with a Hitachi S-530 scanning electron microscope (SEM). The samples were freeze-fractured in liquid nitrogen and sputter-coated with gold. The cell size and cell density were determined from SEM micrographs. The cell diameter is the average of sizes of at least 100 cells on the SEM micrographs. The cell density

(N_0), the number of cells per cubic centimeter of solid polymer, is determined from Eq. (1) [30]:

$$N_0 = \left[\frac{nM^2}{A}\right]^{3/2}\left[\frac{1}{1-V_f}\right] \quad (1)$$

where n is the number of cells on the SEM micrograph, M the magnification factor, A the area of the micrograph (cm^2), and V_f the void fraction of the foamed sample, which can be estimated as

$$V_f = 1 - \frac{\rho_f}{\rho} \quad (2)$$

3. Results and discussion

3.1. Broad distribution of cell sizes in neat PC foams

The as-received PC was melt-processed in the mixer or twin-screw extruder, and then compression molded into the sheet samples. In addition, the as-received PC was also compression molded into the sheet samples directly. These processed PC samples and unprocessed (as-received) PC sample were saturated with $scCO_2$ at 12 MPa and 50 °C for 10 h, and then foamed at 120 °C for 30 s. SEM micrographs of these PC foams are presented in Fig. 1. All the three foams had well-defined closed cell under this condition. The unprocessed PC foam shows a narrow cell size distribution. This typical cell morphology has been observed in PC [31] and other pure polymer microcellular foams [32]. By contrary, the processed PC foams revealed a clear cell structure with broad cell size distribution, which has never been reported on other pure polymer foams. In the following section, the cell morphology evolution of the processed PC foam was investigated by changing the foaming time. Based on these results, a discussion was made on the possible effect of melt-processing on the cell morphology. The PC processed in the mixer was chosen for our study, as both the mixer-processed and extruder-processed PC samples displayed a similar foaming behavior. For simplicity, the processed PC was named as neat PC.

The neat PC after melt-processing in the mixer was saturated with $scCO_2$ under 12 MPa and 50 °C for 10 h, and then foamed at 120 °C for 3–120 s. In Fig. 2 presented are typical SEM micrographs and corresponding cell size distribution of neat PC foams for foaming time of 3 and 120 s, respectively. The foams had well-defined closed cell under these foaming conditions. An important feature of neat PC foams was a quite broad distribution of the cell sizes. At 3 s, just a few cells were observed in the polymeric matrix at a low magnification of ×300. When the magnification was increased to ×2000, the micrograph revealed a clear bimodal cell structure: most cells in neat PC foams are below 2 μm, while a fewer large ones are above 5 μm. The corresponding cell size distribution indicates that both populations occupied the similar volume. With increasing the foaming time, the cell sizes of both populations increased gradually. However, no obvious change in cell size distribution was observed at the foaming time up to 120 s. Therefore, the obvious morphology for these foams indicates that the foaming time was not the primary reason for the broad distribution of cell sizes.

Fig. 3 shows the cell density and expansion ratio of neat PC foams at various foaming times. The cell density of neat PC foams was about 1.10×10^{11} cells/cm^3 for all the seven samples, independent of foaming time. It further indicates that the cell nucleation has been almost completed within 3 s of foaming time, and neither coalescence nor nucleation of cells occurred thereafter. Therefore, the cell density of the foamed sample was taken to represent the corresponding nucleation density in the following discussion. Fig. 3 also shows that the expansion ratio of neat PC foams increases quickly with increasing the foaming time at the time less than 30 s, and then levels off at the time up to 120 s. This result indicates that the cell structure has been developed completely in the first 30 s, and this foaming time was applied in all the following experiments.

In our experiment, the shortest foaming time was 3 s, by taking into account heat transfer process, but this time was enough for the cell nucleation process. The broad size distribution should be formed at the foaming time less than 3 s, and still existed within the time up to 120 s. Therefore, this broadly distributed cell structure did form in the nucleation stage, resulting from the broad cell nucleation process. It has been suggested that the presence of heterogeneous impurities originated from the batch mixer could drastically affect the nucleation rate [20], resulting in the broad cell size distribution.

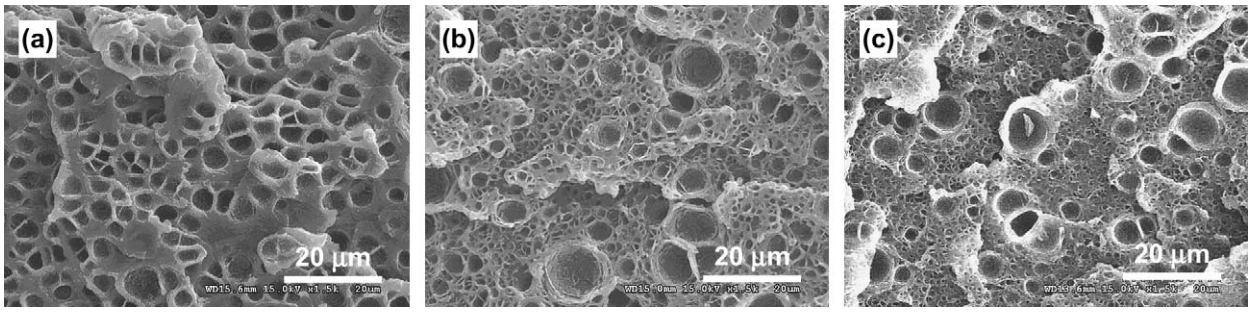

Fig. 1. SEM micrographs illustrating the effect of processing histories on the nucleation behavior of PC saturated at 12 MPa and foamed at 120 °C for 30 s: (a) as-received PC, (b) the processed PC by mixer, and (c) the processed PC by twin-screw extruder.

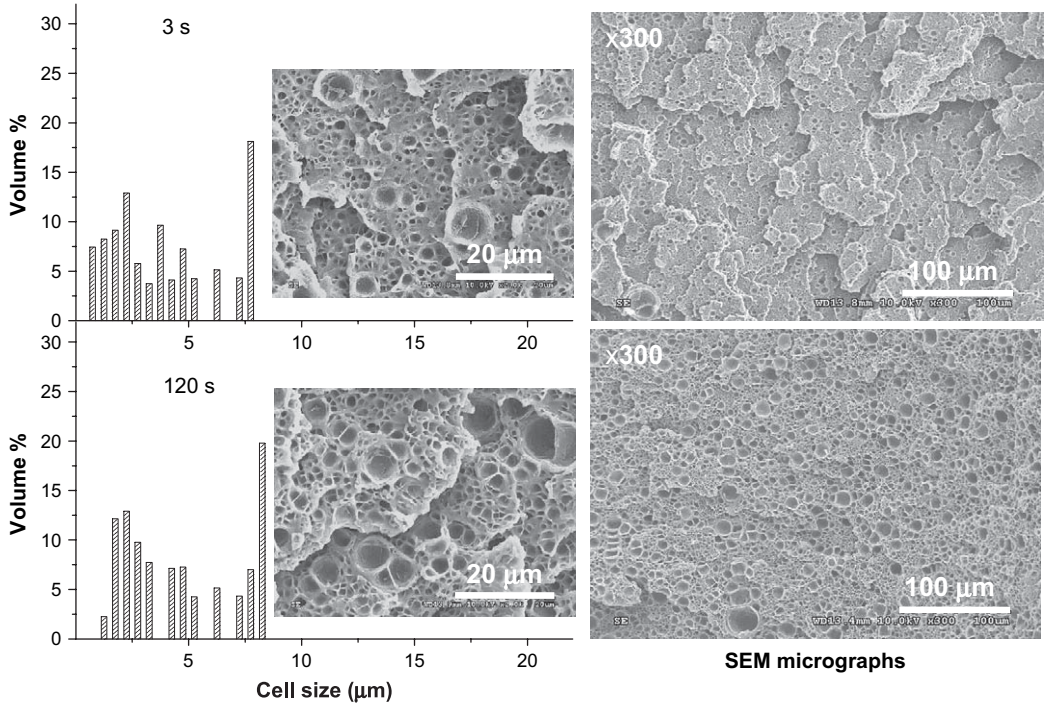

Fig. 2. SEM micrographs and cell size distribution of neat PC foams saturated at 12 MPa and foamed at 120 °C for 3 and 120 s.

In the present study, the influence of dust was avoided by cleaning the mixer three times before melt blending. Therefore, the presence of the broad distribution of cell sizes should be attributed to the melt-processing itself. GPC measurement was used to investigate any possible degradation of PC due to the melt blending, and the results are shown in Fig. 4. The GPC results show an obvious decrease in high molecular weight portion of PC after melt blending. The degradation reaction decreased the molecular weight of PC, which might extend the nucleation process of neat PC in microcellular foaming, and resulted in the broad distributions of cell size. However, more detailed studies are needed to understand the mechanism.

3.2. Effect of nano-silica contents on cell morphology of PCSN foam

In this study, the spherical nano-silica, chosen as the nucleating agent, was compounded with PC matrix via melt-processing. The nano-silica dispersion on PC matrix before foaming was characterized first because of its importance in the morphology of nanocomposite microcellular foam [6–8, 13–20]. Then the effect of nano-silica particle on the cell morphology, especially the cell size distribution, of PCSN foams was investigated based on the classical nucleation theory.

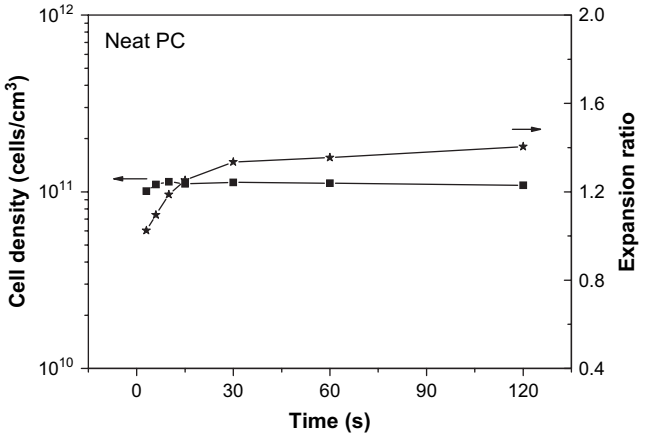

Fig. 3. The cell density and expansion ratio of neat PC foams saturated at 12 MPa and foamed at 120 °C for 3–120 s.

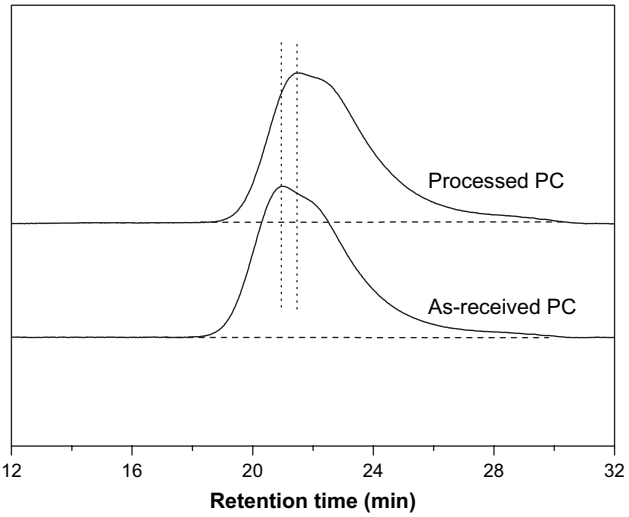

Fig. 4. GPC results of as-received PC and melt-processed PC by mixer (neat PC).

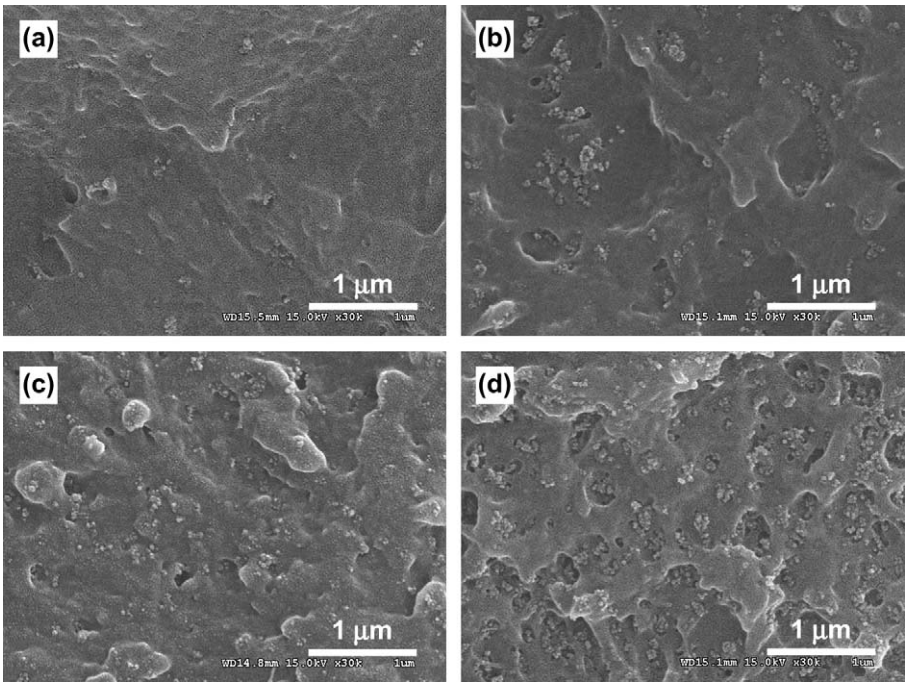

Fig. 5. SEM micrographs of the fractured surfaces of the (a) PCSN1, (b) PCSN3, (c) PCSN5, and (d) PCSN9 samples.

3.2.1. Particle dispersion in PC matrix and PC foam

Fig. 5 shows SEM micrographs of the resultant PCSN samples with different silica contents. It is seen clearly that PCSN9 has plentiful well-scattered multi-silica aggregates after melt compounding. With decreasing the nano-silica content from the master batch, the number of aggregates reduced, while the size and dispersion of aggregates did not change obviously. It indicates that the aggregates in the master batch were not re-dispersed or further aggregated by the dilution processing in the mixer. Although the melt-processing was ineffective to disperse the nano-silica particles individually in PC, the surface modification of nano-silica improved the interaction with polymer, and reduced the aggregate's degree of nano-silica particles in PC. In the present study, TEM was used to show the size of nano-silica aggregate in PCSN9 sample. For comparison, the aggregate's size of foamed PCSN9 sample saturated at 20 MPa and foamed at 120 °C was also observed by TEM. As shown in Fig. 6, the nano-silica aggregates with size of about 50 nm were dispersed uniformly on PCSN9 sample. Consequently, PCSN having well-dispersed silica aggregates were obtained in this study, instead of composites with the silica dispersion at micron-meter scale as usually reported.

3.2.2. Uniform distribution of cell sizes in PCSN foam

In order to study the heterogeneous nucleation effect of nano-sized filler as the nucleating agent, PCSN samples were foamed at 120 °C for 30 s after being saturated at 20 MPa along with neat PC as reference. Fig. 7 shows SEM micrographs and corresponding cell size distribution of foamed samples. All foams exhibit closed spherical or polyhedron cell structures. The neat PC foam also has an obvious broad cell size distribution with cell sizes between 0.7 and 6.0 μm. With the addition of nano-silica into PC matrix, the range of cell size distribution narrowed to 0.2–1.5 μm for PCSN1 foam, 0.2–1.2 μm for PCSN3, 0.1–1.0 μm for PCSN5, and 0.1–0.8 μm for PCSN9. The result indicates that the cell size distribution became more and more uniform with increasing silica content. Moreover, it is noted in Fig. 6 that the distance of adjacent aggregates increased with the foaming process. This phenomenon indicates that the foaming process facilitated the dispersion of aggregates, which is partially attributed to the expansion of PCSN foams.

Fig. 8 summarizes the results of cell structure of foamed samples as a function of silica content, including cell density, cell size, and cell size distribution represented by the standard

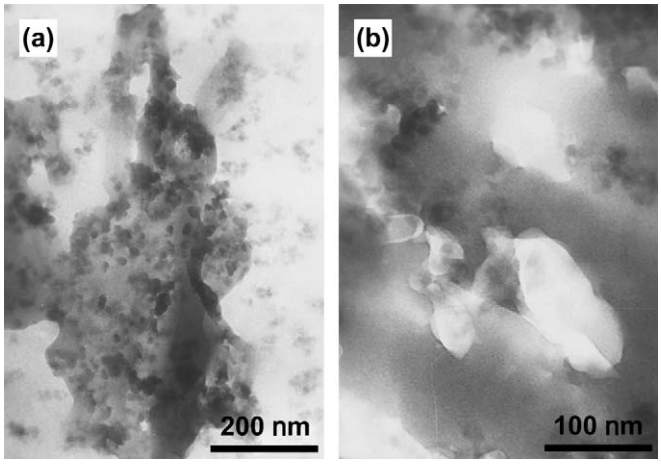

Fig. 6. TEM micrographs of PCSN9 (a) sample and (b) foam saturated at 20 MPa and foamed at 120 °C.

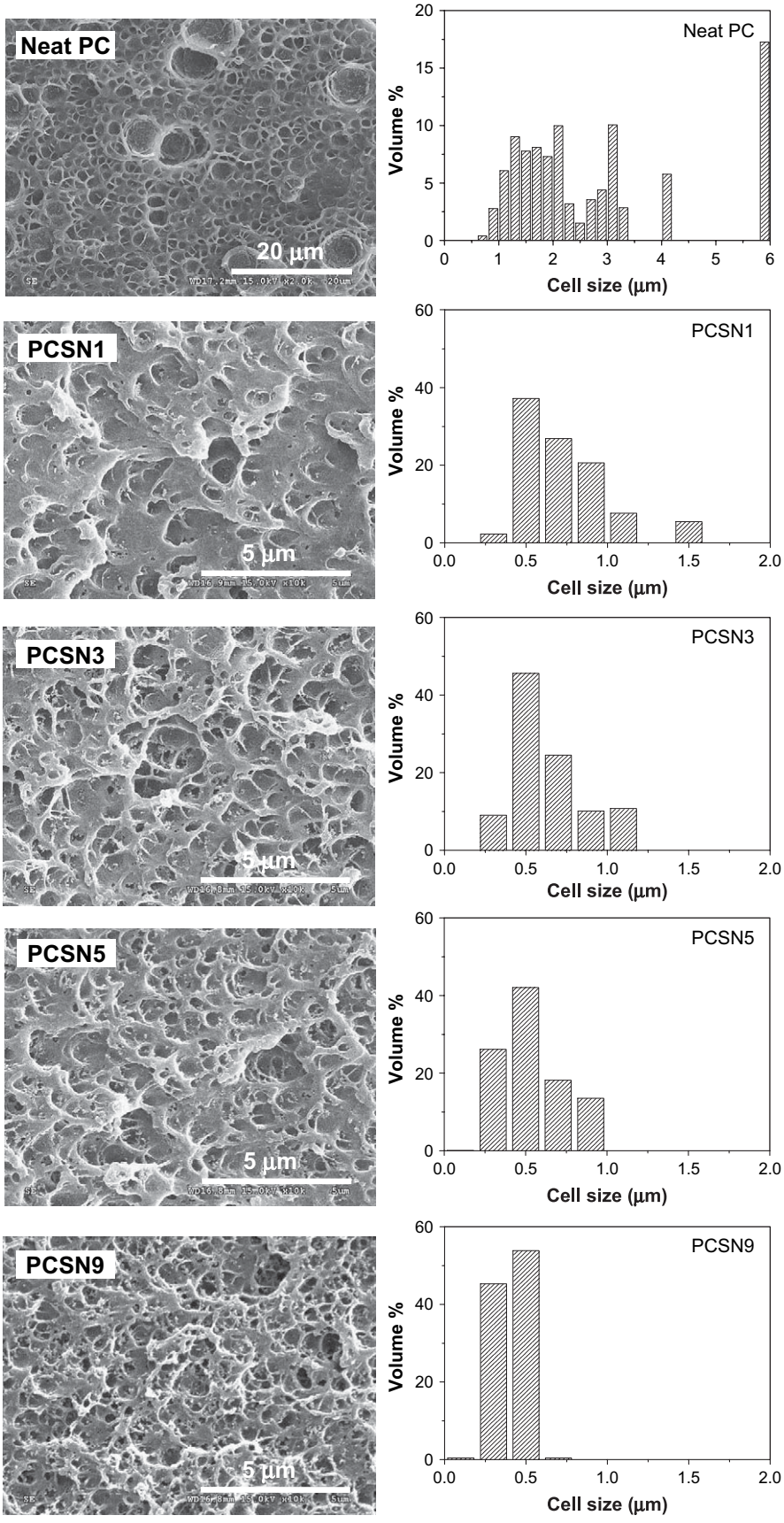

Fig. 7. SEM micrographs and cell size distribution of neat PC and PCSN foams saturated at 20 MPa and foamed at 120 °C for 30 s.

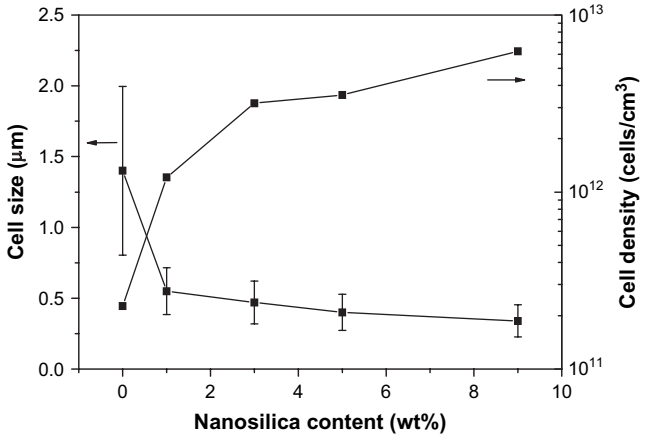

Fig. 8. The cell size and cell density of neat PC and PCSN foams saturated at 20 MPa and foamed at 120 °C for 30 s.

deviation displayed as error bars. It is shown that the average cell diameter decreased remarkably from neat PC foam to PCSN1 with only 1 wt% nano-silica added and then leveled off at higher silica contents. Submicron-sized cells were obtained for foamed PCSN with average cell diameters of 0.55 (PCSN1), 0.47 (PCSN3), 0.40 (PCSN5), and 0.34 μm (PCSN9) compared to 1.40 μm of neat PC foam. The standard deviation of cell sizes decreased obviously for PCSN1 foam by comparison with neat PC foam, and decreased a little with further increase in the nano-silica content within the error range. On the other hand, the cell density increased remarkably from 2.27×10^{11} cells/cm^3 of neat PC foam to 1.21×10^{12} cells/cm^3 of PCSN1 and then slowly increased with further increase in the silica content. For PCSN9 foam, the cell density, 6.25×10^{12} cells/cm^3, was almost five times of that of PCSN1 foam. Compared with microcellular morphology of neat PC foam, those of PCSN foams were improved greatly with the addition of nano-silica up to 9 wt%.

In general, the interface between PC and aggregate is a high energy region resulting from surface effects. In these regions, the Gibbs free energy necessary for nucleating a stable cell is less than that for homogeneous nucleation, resulting in the preferential nucleation of cells at the interface. In PCSN systems, the ratio (f) of Gibbs free energy of heterogeneous (ΔG^*_{het}) nucleation to homogeneous (ΔG^*_{hom}) one was calculated semi-quantitatively by Eqs. (3)–(8) [7,33].

$$f(m,n) = \frac{\Delta G^*_{het}}{\Delta G^*_{hom}} = \frac{1}{2} + \frac{1}{2}\left(\frac{1-mn}{g}\right)^3 + \frac{n^3}{2}\left[2 - 3\left(\frac{n-m}{g}\right) + \left(\frac{n-m}{g}\right)^3\right] + \frac{3}{2}mn^2\left(\frac{n-m}{g} - 1\right) \quad (3)$$

$$\Delta G^*_{hom} = \frac{16\pi\gamma^3}{3\Delta P^2} \quad (4)$$

$$m = \cos\theta \quad (5)$$

$$n = R/r^* \quad (6)$$

$$g = \left(1 + n^2 - 2mn\right)^{1/2} \quad (7)$$

$$r^* = \frac{2\gamma}{\Delta P} \quad (8)$$

where γ is the surface tension at the gas–polymer interface, ΔP the pressure exerted by the $scCO_2$ on the cell walls, θ the polymer-particle-gas contact angle, n the relative curvature of the nucleant surface, R, to the critical radius of the nucleated phase, r^*.

It is very difficult to measure the interfacial tension of polymer/CO_2 at high temperature and high pressure, and no value for PC/CO_2 was reported in the literature. In the present study, the interfacial tension of PC/$scCO_2$, γ_{mix}, was calculated according to Eq. (9) reported by Beckman and Goel [34], where the surface tension of pure $scCO_2$ was defined to be zero.

$$\gamma_{mix} = \gamma_{polymer}\left(\frac{\rho_{mix}}{\rho_{polymer}}\right)^4\left(1 - w_{gas}\right)^4 \quad (9)$$

where $\rho_{polymer}$ and ρ_{mix} are the mass density of polymer and polymer/CO_2 mixture, respectively, and w_{gas} is the weight fraction of CO_2 absorbed in the polymer. The foaming conditions and corresponding literature values of various parameters are listed in Table 1. Therefore, γ_{mix} was calculated to be 17.4 mN/m from Eq. (9), r^* was 1.74 nm from Eq. (8), and hence n was around 3.74 for individual nano-silica particle. With a typical contact angle of 20° [5], Eq. (3) yielded a reduction factor f of 4.93×10^{-3}, which means that the energy required for cell nucleation on the surfaces of nano-silica (ΔG^*_{het}) was only 4.93×10^{-3} of that in homogeneous case (ΔG^*_{hom}). Therefore, the heterogeneous nucleation will be dominant in PCSN microcellular foaming, which is expected to affect the nucleation density of PCSN foam.

The potential nucleation density can be estimated by Eq. (10) [20]:

$$\frac{\text{Nucleants}}{\text{cm}^3} = \frac{w_P}{\rho_P}\frac{\rho_C}{V_P} \quad (10)$$

where w_P is the weight fraction of the particle in the composite, ρ_P and ρ_C are the density of the particle and the polymer

Table 1
The parameters for calculating the $f(m,n)$[a]

w_{gas}[b]	ρ_{mix}[c]	$\gamma_{polymer}$[d]	γ_{mix}	r^*	n[e]
10 wt%	1.11 g/cm^3	36.3 mN/m	17.4 mN/m	1.74 nm	3.74

[a] Foaming condition: saturation temperature, 50 °C; saturation pressure, 20 MPa; and foaming temperature, 120 °C.
[b] Obtained from Ref. [35].
[c] Obtained from Ref. [36].
[d] Calculated according to Ref. [37] at ambient pressure and 120 °C.
[e] Calculated from Eq. (6), where R is the average radius (6 nm) of individual nano-silica particle.

Table 2
A comparison of potential nucleant density and actual cell density

Nanocomposite	Content of nanoparticle (wt%)	Potential nucleation density[a] (cells/cm^3)	Measured nucleation density (cells/cm^3)	Efficiency (%)
PCSN1	1	6.63×10^{15}	1.21×10^{12}	1.83×10^{-2}
PCSN3	3	1.99×10^{16}	3.17×10^{12}	1.59×10^{-2}
PCSN5	5	3.32×10^{16}	3.54×10^{12}	1.07×10^{-2}
PCSN9	9	5.97×10^{16}	6.25×10^{12}	1.05×10^{-2}
PS/SWCNT[b]	0.1	1.59×10^{15}	1.44×10^{9}	9.06×10^{-5}

[a] Calculated from Eq. (10) with the assumption of complete particle dispersion.
[b] Polystyrene/single wall carbon nanotube nanocomposite [10].

composite, respectively, and V_P is the volume of the individual particle. According to Eq. (10), the potential nucleation density of PCSN1 was 6.63×10^{15} cells/cm^3 (calculated by individual nano-silica particle). After microcellular foaming at 120 °C with saturation pressure of 20 MPa, the cell density of PCSN1 foam was 1.21×10^{12} cells/cm^3. The nucleation efficiency of silica, defined by the ratio of measured cell density to the potential nucleant density, was 1.83×10^{-2}%. Similar calculations were conducted for other PCSN samples and the results are listed in Table 2. As shown in Table 2, the nucleation efficiency of silica particles was about 1.00×10^{-2}%, and did not obviously decreases with increasing the silica loading, which might be attributed to the unchanged aggregate's size and the interfacial properties between PC and aggregate. The obvious aggregate of silica in PC matrix reduced the actual potential nucleation density, hence decreased the measured nucleation density and the benefit of heterogeneous nucleation. In other nanocomposites, the nucleation efficiency of nanoparticles was also low [10].

It is established that the final cell size distribution depends on nucleation rate along with cell growth dynamics. Any change in the parameter which increases the nucleation rate or decreases the cell growth rate will narrow cell size distribution [23]. For PCSN samples, the melt-processing in the mixer also affected the polymer characteristics such as molecular weight, thus the broad cell size distribution should be observed in the final foams. Due to the presence of nano-silica aggregates, however, the cell nucleation behavior of PCSN showed an obvious change. The silica aggregates dispersed uniformly on PC matrix had the similar size of about 50 nm, irrespective of nano-silica loading. The nuclei would be activated by these nucleation sites with a high nucleation rate due to the low

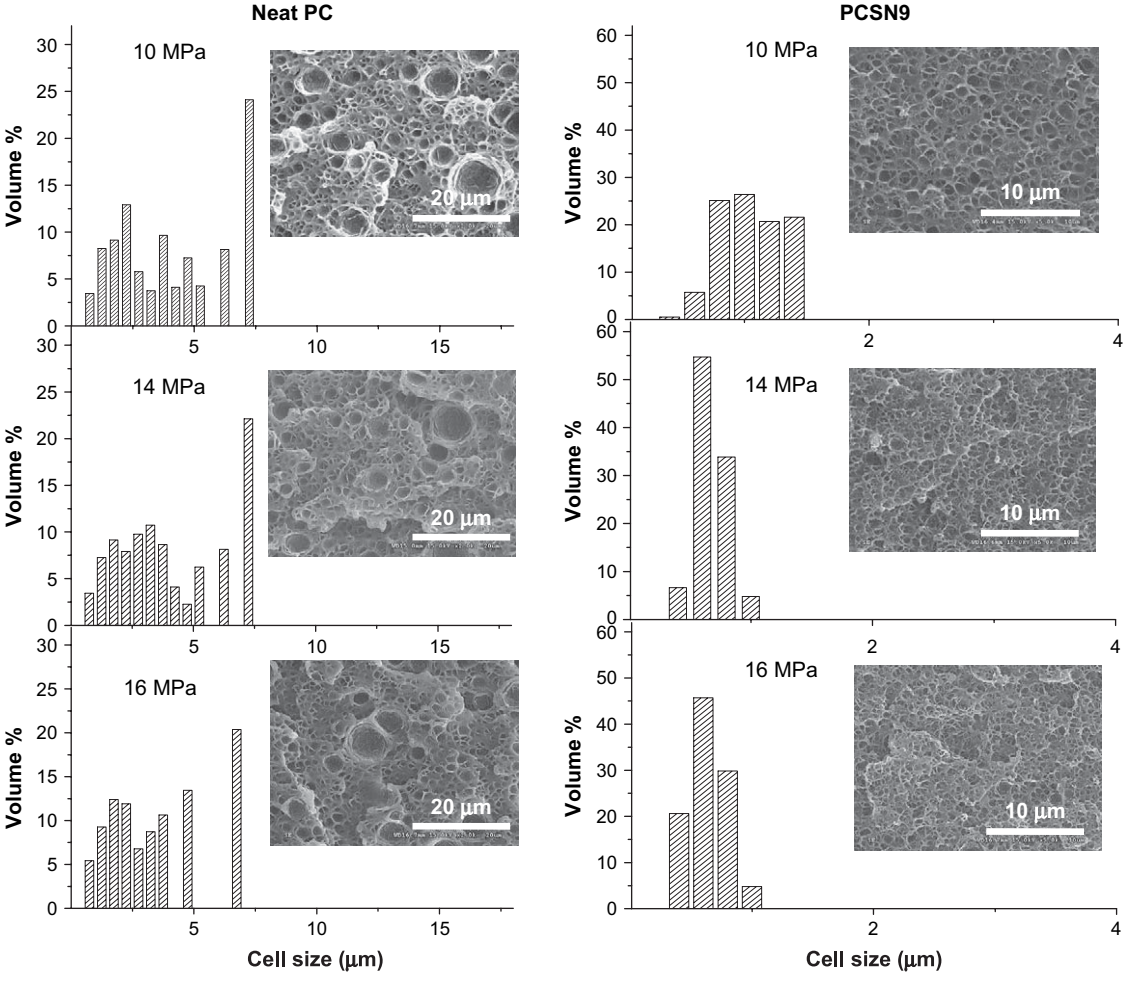

Fig. 9. SEM micrographs and cell size distribution of neat PC and PCSN9 foams saturated at various pressures and foamed at 120 °C for 30 s.

ΔG^*_{het}. Meanwhile, those nuclei tended to disperse uniformly on the polymeric matrix due to the well-dispersed nucleation sites, which was the precondition to form the uniform cell size distribution in PCSN foams. An increase in nucleation rate of primary nucleation process depleted most of the blowing agents, which inhibited the secondary cell nucleation. It means that the time interval for cell nucleation was shortened dramatically. Therefore, the formed nuclei grew almost instantaneously during the foaming process. On the other hand, less amount of CO_2 was left for cell growth, because most of the CO_2 was consumed in the cell nucleation. Consequently, both the size and the size distribution decreased for the final foams. In this study, this effect of nano-silica content worked up to 9 wt% because of similar dispersion and size of potential nucleation sites for these nanocomposites. In conclusion, the uniform distribution of nucleation sites and the energy-favored heterogeneous nucleation counterbalanced the factors resulting in the broad size distribution in neat PC foam to a certain extent.

3.3. Effect of saturation pressure and foaming temperature on cell morphology

Fig. 9 shows the SEM micrographs and corresponding cell size distribution of the foamed neat PC and PCSN9 samples obtained with the saturation pressure varying from 10 to 16 MPa, at foaming temperature of 120 °C. The neat PC foams also had an obvious broad cell size distribution under these foaming conditions. However, with increasing the saturation pressure, the range of sizes became a little narrower from 0.8–7.3 μm at 10 MPa to 0.8–7.3 μm at 14 MPa, and to 0.8–6.8 μm at 16 MPa. The addition of nano-silica into PC matrix significantly affected the cell size distribution of PCSN foams. A normal distribution of cell sizes was observed for PCSN9 foams, and the range of sizes was 0.4–1.4 (10 MPa), 0.4–1.0 (14 MPa), and 0.4–1.0 μm (16 MPa). It indicates that increasing the saturation pressure tended to narrow the cell size distribution of PCSN9 foams as well. According to Eq. (4), the increase of saturation pressure decreased the ΔG, increased the nucleation rate for nucleation, shortened the time for cell nucleation, and hence helped to narrow the cell size distribution of neat PC and PCSN foams. Fig. 9 also shows that the cell size distribution of PCSN9 foam was more sensitive to the saturation pressure, compared to neat PC foam. A possible reason was that the increased saturation pressure decreased $f(m,n)$ (according to Eq. (3, 5–8)) along with ΔG^*_{hom}, and further decreased the ΔG^*_{het}, and hence showed a significant increase in heterogeneous nucleation rate.

Foaming temperature is another factor which affects the cell morphology of polymer foams. Fig. 10 shows the cell density of the neat PC and PCSN foams obtained at different foaming temperatures from 100 to 150 °C after saturation at 12 MPa and 50 °C. The increase of temperature decreases the cell density of the neat PC foam especially at the foaming temperature of 150 °C, but has little effect on the nucleation of nanocomposites. The addition of inorganic nano-sized fillers increased the elastic modulus of polymer nanocomposites

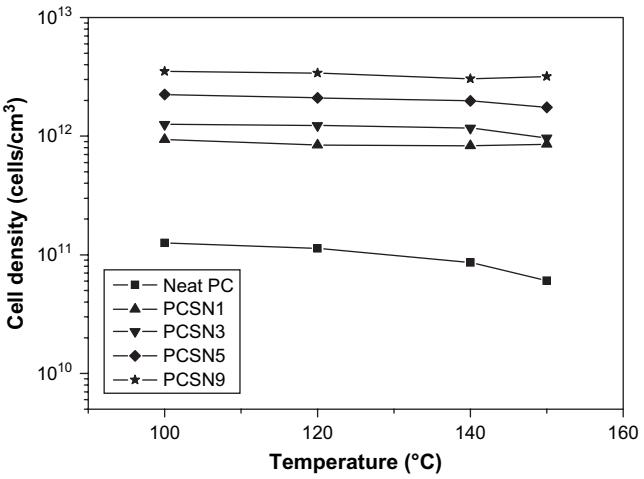

Fig. 10. Plot of the cell density of neat PC and PCSN foams as a function of foaming temperature. Samples were saturated at 12 MPa and foamed for 30 s.

matrix [16], and served as internal diffusion barriers to retard the CO_2 escape during foaming [17,38], which would decrease the influence of foaming temperature on the cell density to a certain extent.

4. Conclusions

In the present paper, microcellular neat PC and PC/nano-silica nanocomposites were prepared by using a temperature rising process with supercritical CO_2 as the blowing agent. The results revealed that the neat PC showed a broad distribution of cell size after foaming, while the foamed PCSN had uniform distribution of cell sizes with average values of 0.3–0.5 μm. The nano-silica aggregates served as an effective nucleating agent inducing the energy-favorable heterogeneous nucleation, which tended to activate the instantaneous nucleation and uniform growth. Combining with the uniform dispersion in PC matrix, nano-silica aggregates facilitated the uniform distribution of cell size in PCSN foams. Therefore, the theory of heterogeneous nucleation [9] was confirmed experimentally from the aspect of cell size distribution. An increase in the saturation pressure tended to narrow the cell size distribution and to increase the cell density of neat PC and PCSN foams, because the enhanced CO_2 concentration at high saturation pressure shortened the period of time for cell nucleation. In addition, the foaming temperature did not affect the cell density of PCSN foams due to the dominant heterogeneous nucleation. Meanwhile, the heterogeneous nucleation mechanism dominating the microcellular foaming of PCSN also determined the remarkable increase of cell density and decrease of cell size with increasing nano-silica content.

Acknowledgement

This work was supported by the Innovation Funds of CAS.

References

[1] Klempner D, Frisch KC. Handbook of polymeric foams and foam technology. New York: Oxford University Press; 1991.
[2] Martini JE, Waldman FA, Suh NP. SPE ANTEC Tech Pap 1982;1:674–6.
[3] Park CB, Cheung LK, Song SW. Cell Polym 1998;17:221–51.
[4] Yang HH, Han CD. J Appl Polym Sci 1984;29:4465–70.
[5] Colton JS, Suh NP. Polym Eng Sci 1987;27:485–92.
[6] Colton JS, Suh NP. Polym Eng Sci 1987;27:493–9.
[7] Colton JS, Suh NP. Polym Eng Sci 1987;27:500–3.
[8] Wang J, Cheng XG, Yuan MJ, He JS. Polymer 2001;42:8265–75.
[9] McClurg RB. Chem Eng Sci 2004;59:5779–86.
[10] Shen J, Zeng C, Lee LJ. Polymer 2005;46:5218–24.
[11] Han X, Zeng C, Lee LJ, Koelling KW, Tomasko DL. Polym Eng Sci 2003;43:1261–75.
[12] Zeng C, Han X, Lee LJ, Koelling KW, Tomasko DL. Adv Mater 2003;15:1743–7.
[13] Okamoto M, Nam PH, Maiti P, Kotaka T, Hasegawa N, Usuki A. Nano Lett 2001;1:295–8.
[14] Mitsunaga M, Ito Y, Ray SS, Okamoto M, Hironaka K. Macromol Mater Eng 2003;288:543–8.
[15] Cao X, Lee LJ, Widya T, Macosko C. Polymer 2005;46:775–83.
[16] Di YW, Iannace S, Maio ED, Nicolais L. J Polym Sci Part B Polym Phys 2005;43:689–98.
[17] Chandra A, Gong S, Yuan M, Turng LS. Polym Eng Sci 2005;45:52–61.
[18] Lee LJ, Zeng C, Cao X, Han X, Shen J, Xu G. Compos Sci Technol 2005;65:2344–63.
[19] Siripurapu S, DeSimone JM, Khan SA, Spontak RJ. Macromolecules 2005;38:2271–80.
[20] Spitael P, Macosko CW, McClurg RB. Macromolecules 2004;37:6874–82.
[21] Mao D, Edwards JR, Harvey A. Chem Eng Sci 2006;61:1836–45.
[22] Kumar V. Colloids Surf A 2005;263:336–40.
[23] Shafi MA, Joshi K, Flumerfelt RW. Chem Eng Sci 1997;52:635–44.
[24] Feng JJ, Bertelo CA. J Rheol 2004;48:439–62.
[25] Gross SM, Roberts GW, Kiserow DJ, Desimone JM. Macromolecules 2000;33:40–5.
[26] Liao X, Wang J, Li G, He JS. J Polym Sci Part B Polym Phys 2004;42:280–5.
[27] Beckman E, Porter RS. J Polym Sci Part B Polym Phys 1987;25:1511–7.
[28] Doroudiani S, Park CB, Korschot MT. Polym Eng Sci 1996;36:2645–62.
[29] Baldwin DF, Shimbo M, Suh NP. J Eng Mater Technol 1995;117:62–74.
[30] Kumar V, Suh NP. Polym Eng Sci 1990;30:1323–9.
[31] Kumar V, Weller J. J Eng Ind 1994;116:413–20.
[32] Arora KA, Lesser AJ, McCarthy TJ. Macromolecules 1998;31:4614–20.
[33] Fletcher NH. J Chem Phys 1958;29:572–6.
[34] Goel SK, Beckman EJ. AIChE J 1995;41:357–67.
[35] Tang M, Du TB, Chen YP. J Supercrit Fluids 2004;28:207–18.
[36] Li G, Wang J, Park CB, Simha R. PPS20 foam symposium; 2004.
[37] Hobbs SY, Dekkers MEJ, Watkins VH. Polymer 1988;29:1598–602.
[38] Siripurapu S, DeSimone JM, Khan SA, Spontak RJ. Adv Mater 2004;16:989–94.